

# On Aerodynamic Modelling for Rotorcraft Flight Dynamics\*

Bruce D. Kothmann

Jeffrey D. Keller

H. C. Curtiss, Jr.

Princeton University  
Princeton, New Jersey USA

## Abstract

It has been known for some time that the prediction of rotor forces and moments for flight dynamics applications is sensitive to the specific assumptions employed in modelling aerodynamics. This paper reviews several critical aspects of the most widely used models and the suggested extensions to them, with an emphasis on the prediction of helicopter control response.

## 1 Nomenclature

$\mathcal{R}$	fixed wing aspect ratio
$B$	tip loss factor (0.97)
$C$	lift deficiency function
$C_L$	aerodynamic roll moment coefficient
$C_M$	aerodynamic pitch moment coefficient
$C_T$	thrust coefficient
$c$	normalized wing chord
$e_A$	normalized blade inner radius
$[J]$	inflow momentum flux matrix
$K_c(\chi)$	wake skew function
$\bar{K}_c$	$K_c$ in edgewise flow ( $K_c(90^\circ)$ )
$K_T$	wake translational deformation parameter
$K_R$	wake rotational deformation parameter
$K_\beta$	normalized hub spring
$[M]$	inflow added mass matrix
$N$	wake rigidity factor
$V$	normalized flight speed
$V_G$	Glauert mass flow parameter
$V_{mass}$	generalized mass flow parameter
$\alpha$	disc angle of attack, positive for rearward tilt
$\alpha_G$	geometric angle of attack
$\alpha_o$	net 2D angle of attack
$\alpha_{i2D}$	2D induced angle of attack
$\alpha_{i3D}$	3D induced angle of attack
$\Gamma$	bound circulation
$\Gamma_k$	$k$ -th aerodynamic integral
$\gamma_i$	Pitt model parameter
$\lambda$	inflow ratio, $V \sin \alpha - \nu_o$
$\mu$	advance ratio, $V \cos \alpha$

$\nu$	normalized inflow velocity $\nu = \nu_o + \nu_s \frac{r}{R} \sin \psi + \nu_c \frac{r}{R} \cos \psi$
$\sigma$	rotor solidity
$\tau$	inflow time constant
$\chi$	wake skew angle
$\omega$	normalized frequency

## 2 Introduction

This paper considers the influence of various aerodynamic modelling assumptions on the prediction of the control response of single-rotor helicopters. In contrast to aerodynamic models for performance calculations, flight dynamics models are not generally expected to accurately capture all of the details of the complex flow of a lifting rotor. Flight dynamics applications, which by nature involve unsteady fuselage motion and non-periodic rotor dynamics, continue to present an unmanageable challenge to the most sophisticated numerical analyses. Therefore, we will be satisfied with models which offer a compelling analytical basis, and may be expected to provide an accurate representation of a physical phenomenon. In addition, there should be as few adjustable parameters as possible, with a clear understanding of the factors which influence their values, to provide a quantitative description of the integrated effect of the phenomenon.

Classically, there are two distinct and equally important aspects to the aerodynamic modelling for flight dynamics: (i) computing the airload at a particular blade station as a function of the local air velocity and blade motion; and (ii) computing the flow induced by a rotor which is generating aerodynamic forces and moments. In most flight dynamics analyses, linear, quasi-steady strip theory comprises the former, while momentum theory and/or dynamic inflow comprise the latter. The dominant physical characteristics of the rotor response are well represented by these theories and their simplicity provides valuable insight. However, the completeness of these theories has been called into question by the need for unrealistic parameter values to match experimental

\*Presented at the 22nd European Rotorcraft Forum, September, 1996, Brighton, UK. This work was supported by NASA Ames Research Center, Grant NAG 2-561.

data, especially for the off-axis response to control inputs, in recent system identification studies [1, 2]. Therefore, the need for fundamental investigations of these theories continues.

### 3 Unsteady Aerodynamics

This section explores the relationship between vortex and unsteady momentum theories with the goal of clarifying the aforementioned conceptual division between predicting unsteady loads and induced velocity. In order to achieve the desired insight, it is most useful to consider the theories applied to a fixed wing. The conclusions for the fixed-wing case are directly applicable to the rotating wing for collective pitch inputs. Although the concepts are roughly the same, the wake geometry of a rotor renders the response to cyclic inputs considerably more challenging, and we delay explicit consideration of this case to Section 5. Note that all variables in this section have been normalized on density, the flight speed, and the span of the wing.

Figure 1 shows a block diagram expressing the relationship between the geometric angle of attack and the lift for a finite wing, from the perspective of unsteady vortex theory. (The results are approximate as the wing is assumed to be elliptical and the details of the spanwise distribution of circulation and lift are omitted.) The enforcement of the Kutta condition results in the static relationship between the total angle of attack and the wing circulation. The two-dimensional (2D) dynamic feedback of circulation, given in Laplace domain by  $H_2(s)$ , represents the 2D induced angle of attack due the spanwise vorticity shed into the wake, as described by Theodorsen [3] and von Karman and Sears [4, 5]. The three-dimensional (3D) dynamic feedback of circulation,  $H_3(s)$ , represents the dynamics of the streamwise tip vortices which trail a finite wing, as discussed by Jones [6]. Finally, the relationship between circulation and lift,  $H_1(s)$ , results from using the unsteady velocities to find the unsteady pressure distribution (i.e. the unsteady Bernoulli equation). It should be noted that the two-dimensional added-mass terms have been neglected in this description.

The transfer functions,  $H_1$ ,  $H_2$ , and  $H_3$  are quite complicated, generally involving Bessel functions, and have been given in various forms in the above cited literature. For the present purposes, it will suffice to indicate crude approximations to these functions which produce the correct qualitative behavior. Because the effects of the shed wake should vanish in steady state for the 2D case, we must have  $H_2(s) \rightarrow 0$

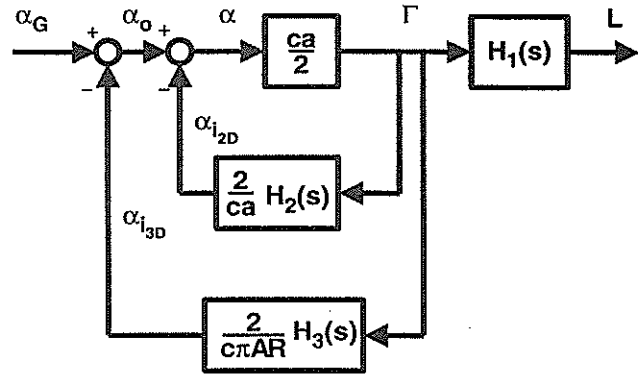


Figure 1: Block Diagram of Unsteady Vortex Theory for Finite Fixed Wing

$H_1(s)$	$H_2(s)$	$H_3(s)$
$\tau_1 s + 1$	$\tau_2 s$	$\frac{1}{\tau_3 s + 1}$

Table 1: Approximations to Aerodynamic Transfer Functions

as  $s \rightarrow 0$ . In addition, the 2D closed-loop response of  $\Gamma$  to  $\alpha_o$  should roughly appear as a first-order system. Thus, we may take  $H_2(s) \approx \tau_2 s$ , and, because the 2D unsteadiness is governed by the convection of the shed vorticity, we expect the value of  $\tau_2$  to scale with  $c$ . In steady state, the relationship between circulation and lift must approach the well-known Kutta-Joukowski theorem, implying that  $H_1(s) \rightarrow 1$  as  $s \rightarrow 0$ . Also,  $H_1$  must introduce a lead in the lift for non-zero frequencies. Thus, we take  $H_1 \approx \tau_1 s + 1$ , and from the more detailed theories we expect the value of  $\tau_1$  to be about  $\frac{1}{2}$  the value of  $\tau_2$ . Finally, the 3D feedback dynamics may be represented as a simple first-order lag, corresponding to the delayed buildup of the finite-wing induced velocities as the trailing vortices convect downstream. We take  $H_3(s) \approx 1/(\tau_3 s + 1)$ , and expect that  $\tau_3$  will be on the order of 1 (since the convection time of the trailing vortices should scale with wing span and the inverse of freestream speed). These relationships are summarized in Table 1.

The block diagram of Figure 1 can be rearranged to allow a more conventional interpretation, commonly referred to as the momentum (actuator disc) theory, as shown in Figure 2. From this point of view, the lift is directly responsible for the generation of the three-dimensional downwash, represented by the feedback block, and there is an unsteady relationship between the effective 2D angle of attack,  $\alpha_o$ , and the lift. Provided the appropriate transfer functions are used in each of these separate blocks, the momen-

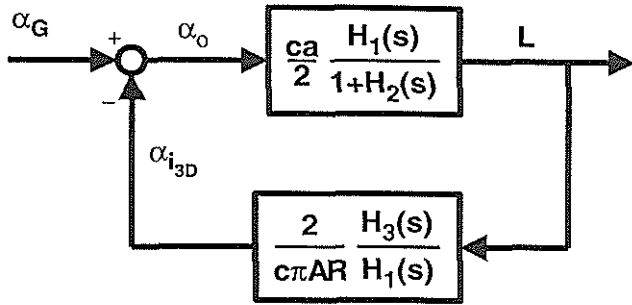


Figure 2: Block Diagram of Actuator Disc (Momentum) Theory for Finite Fixed Wing

tum perspective is exactly equivalent to the vortex theory. Note, though, that dynamic inflow is clearly phenomenologically distinct from the unsteady relationship between angle of attack and lift.

Using the foregoing approximate expressions, the complete transfer function from geometric angle of attack to lift is given by

$$\frac{2L}{\alpha\alpha_G} = \frac{(\tau_3 s + 1)(\tau_1 s + 1)}{(\tau_3 s + 1)(\tau_2 s + 1) + \frac{a}{\pi AR}} \quad (1)$$

with the corresponding time response of lift to a step input in  $\alpha_G$  shown in Figure 3. The response is characterized by an initial jump equal to  $\frac{1}{2}$  of the 2D steady value, followed by a rapid increase, due to the dynamics of the 2D shed vorticity, and finally by a relatively slow decay, due to the dynamics of the 3D trailing vorticity. In light of the fact that  $\tau_2$  (and also  $\tau_1$ ) are much less than  $\tau_3$ , by approximately a factor of  $c$ , which is about one order of magnitude for typical aspect ratios, the theory is often simplified by setting  $\tau_1$  and  $\tau_2$  identically to zero. In this case, the forward block in Figure 2 becomes a static relationship (“quasi-steady strip theory”) and the feedback block becomes the usual first-order dynamic inflow (“unsteady momentum”) theory. This approximation, which is very widely used in flight dynamics, yields a step response as shown in Figure 3. Thus, we see that the usual model is in fact a low-frequency approximation which captures the dominant dynamics of the lift response, neglecting only a small lag in the response due to 2D shed wake effects.

Although the incompressible theory applied to a typical rotor blade suggests that  $\tau_2$  will be quite small, there is evidence [7, 8] that  $\tau_2$  increases with Mach number. In that case, the 2D shed wake effects may introduce enough of a time lag in the lift response to be relevant in rotorcraft flight dynamics analyses. See [1] for evidence that such a lag seems to be present in the off-axis response of recent flight test data. Appropriate modelling of the 2D time-lag effect

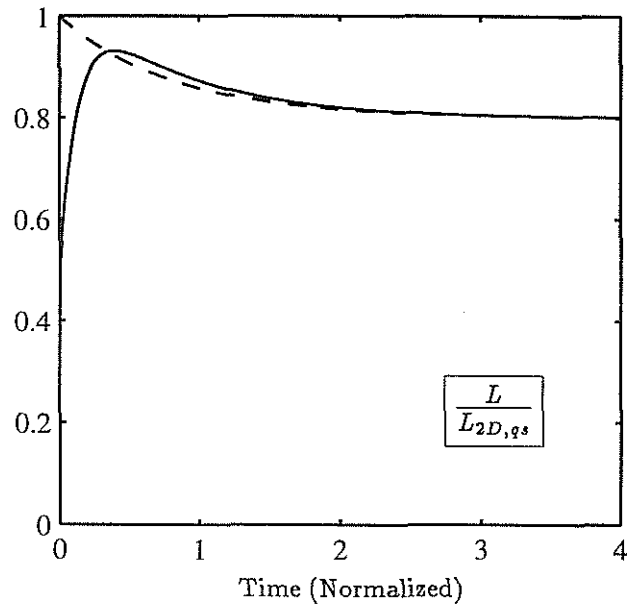


Figure 3: Time Response of Lift to Step Increase in Geometric Angle of Attack ( $AR = 8$ ). Solid = Complete Theory; Dashed = Neglecting 2D Unsteadiness

for flight dynamics applications is being investigated further.

Having justified the conceptual division of aerodynamic modelling into the distinct problems of calculating unsteady loads and induced velocity, we now turn attention to a detailed examination of the current state-of-the-art of the latter.

## 4 Dynamic Inflow Modelling

This section presents a brief survey of the developments in theory and applications which ultimately led to the most widely used dynamic inflow model, originally reported in [9], hereafter referred to as “the Pitt model.” The review is not intended to be comprehensive, nor are we especially concerned here with the historical context, but rather attempt a pointed, critical examination of the theoretical basis of the current inflow theories. Historical information and additional comparisons to test data are in [10], from which selected conclusions will be drawn.

### 4.1 Inflow Terminology

As defined in Section 1, all quantities here follow [11, Appendix I], except that all dimensional quantities have been normalized on  $\Omega R$ . In particular, note the sign convention for the disc angle of attack,  $\alpha$ , and the definition of the inflow ratio,  $\lambda \equiv V \sin \alpha - \nu_o$ .

Much of the theory to follow relies on the notion of the “rotor disc,” a concept which is seldom precisely defined. A consistent choice for the rotor disc is the tip-path plane, because the behavior of a centrally hinged, fully articulated rotor is invariant under changes in tip-path plane tilt in hover [12]. The plane normal to the shaft is an improper choice.

Note that the algebraic complexity of coupling inflow variations to the equations for the blade motion is greatly reduced if the inflow is assumed to be normal to the local blade span, rather than normal to the tip-path plane. (This simplification does not alter the aforementioned invariance.)

## 4.2 Shaft-Fixed Results

Most of the analytical work concerning the flow induced by a rotor producing aerodynamic forces and moments presumes the rotor to be in a steady translational flight condition, which is analogous to a shaft-fixed rotor operating in a wind tunnel. These analyses are conveniently grouped into the axial and non-axial flight cases.

### 4.2.1 Axial Flight: Theory

For a rotor in axial flight, it is possible to perform a convincing analysis based on a control volume formulation, with the axisymmetry of the wake allowing either of 2 well-defined control volumes to be chosen (see [13, 14]). The resulting equations can be put in the following form<sup>1</sup>

$$[M] \begin{pmatrix} \dot{\nu}_o \\ \dot{\nu}_s \\ \dot{\nu}_c \end{pmatrix} + [J] \begin{pmatrix} \nu_o \\ \nu_s \\ \nu_c \end{pmatrix} = \begin{pmatrix} C_T \\ C_L \\ C_M \end{pmatrix} \quad (2)$$

The first term represents the acceleration (angular acceleration for the harmonics) of the fluid within the control volume. The numerical values of the added mass matrix,  $[M]$ , cannot be evaluated by the control volume formulation; typically, the added mass values for an impermeable disc are used:

$$[M] = \begin{bmatrix} \frac{8}{3\pi} & 0 & 0 \\ 0 & -\frac{16}{45\pi} & 0 \\ 0 & 0 & -\frac{16}{45\pi} \end{bmatrix} \quad (3)$$

While these values are an appropriate linearization for the case of a non-lifting, hovering rotor, “the analogy with the accelerating impermeable disc is not strictly valid after a slipstream has formed” [15]. Nevertheless, a credible adjustment of the mass terms

<sup>1</sup>Note that this equation is nonlinear if  $[J]$  depends on  $\nu_o$ .

in the presence of the slipstream has yet to be proposed. (The “corrected” mass matrix presented in [9] is also based on a linearization for zero lift in hover, but with a different pressure distribution than the impermeable disc.)

The second term in Equation (2) accounts for the flux of momentum (and angular momentum) across the boundaries of the control volume, with  $[J]$  given by:

$$[J] = V_{mass} \begin{bmatrix} 2 & 0 & 0 \\ 0 & -\frac{N}{2} & 0 \\ 0 & 0 & -\frac{N}{2} \end{bmatrix} \quad (4)$$

where  $V_{mass} = -\lambda$  in axial flight. The wake rigidity factor,  $N$ , has a value between 1 (rigid wake) and 2 (non-rigid wake). The “rigidity” of the wake actually depends on whether the harmonics are included in expressing the mass flow through the disc. It should be noted that the multiplier of  $N$  ( $\frac{1}{2}$  in Equation (4)) depends on the assumed radial distribution of the harmonic inflow (here linear), so it is perhaps best to regard  $N$  as a parameter whose precise value is to be established by experiments or more elaborate analyses.

The terms on the right-hand side of Equation (2), representing the thrust and aerodynamic moments generated by the rotor, couple the inflow equations to a particular application through the modelling of the rotor aerodynamic loads.

### 4.2.2 Axial Flight: Applications

In hover, steady uniform inflow reduces the thrust produced by application of collective pitch. In the dynamic case, for example following a step input in collective, the time delay in the build up of the inflow causes a delay in this thrust reduction, resulting in an overshoot of thrust relative to the steady value (see the dashed line in Figure 3). In addition, it can be shown that unsteady uniform inflow generally reduces both the natural frequency and the damping ratio of the collective flapping mode, by amounts which depend on the disc loading of the rotor.

An early evaluation of the influence of unsteady uniform inflow is presented in [15], which includes a concise theoretical exposition and measured values of collective flapping, thrust, and induced velocity in response to a variety of rapid collective pitch inputs. While the predicted flapping and thrust show generally very good agreement, the predicted response of the inflow to the sudden loading is faster than the measured response. Because the paper presents only the ratio of the inflow to its steady value, it is not possible to precisely identify the source of the discrepancy, although it suggests that the added mass

term is too small. Note also that [15] includes  $\frac{2}{3}\dot{a}_o$  in  $V_{mass}$ , under the assumption that the rotor disc is attached to the blades at the  $\frac{2}{3}$ -radius point. The consequences of this assumption are a further decrease of about five percent in the collective flap natural frequency and damping ratio. These small changes are not clearly observable in the data, so the validity of this assumption remains unsubstantiated.

The effects of steady harmonic inflow components in axial flight were examined analytically in [16]. The inflow variations alter the flapping response to control inputs, with the magnitude of the change increasing with the first flapping frequency (there is no change for a centrally hinged rotor). The effects can be represented by a modified (or “reduced”) Lock number, so that the pitch and roll damping of the rotor would also be expected to change. Comparisons between the theory and test data for a rigid propeller in hover at several thrust levels clearly demonstrate the importance of the harmonic inflow variations, and the ability of the static momentum theory, with  $N = 2$ , to account for the effects.

Finally, we consider experimental evaluation of the added mass terms for the harmonic inflow in axial flight. A series of papers [17, 18, 19, 20] provides convincing evidence for the importance of these terms. Parameter identification was used to match the measured response of blade flapping to unsteady pitch inputs with the calculations, which included dynamic harmonic inflow in the form of Equation (2). The identified parameters corresponded to the added mass and the wake rigidity factor in the present formulation. The clearest exposition, including precise definitions of the notation, is given in [19], where the identified values are shown to be in close agreement to the theoretical values<sup>2</sup>. In particular, the added mass matrix is well represented by Equation (3) and the wake rigidity factor is shown to be about  $N = 2$ .

#### 4.2.3 Non-Axial Flight: Theory

When the rotor is in non-axial flight, it is no longer possible to define a satisfactory control volume, and the preceding momentum analysis is difficult to extend in a comparably rigorous fashion. Qualitatively, we may expect the equations to have the same form, with the mass flow governed by  $V$  in high-speed forward flight. Based on this notion, Glauert proposed

<sup>2</sup>The identified values correspond closely to the theoretical values only when the measured values of  $\nu_o$  are used. Steady momentum theory overpredicts  $\nu_o$  (given in Table 3 of the reference) by about a factor of two, probably due to the proximity of the rotor to the ground. It is therefore somewhat less than completely satisfying that the momentum theory applies without a ground-effect correction in the dynamic case.

that mass flow in an arbitrary flight condition be calculated using

$$V_G \equiv \sqrt{\mu^2 + \lambda^2} \quad (5)$$

Although this expression cannot be rigorously justified, it does give the correct limiting values, including consistency with the vortex theory for the velocity induced by a non-rotating wing. Therefore, Equation (2), with  $V_{mass}$  in Equation (4) replaced by  $V_G$ , is widely referred to as “momentum theory,” a label which we will maintain. Note that the wake will become “rigid” ( $N = 1$ ) in forward flight, as the mass flux is nearly independent of the induced velocity.

Of course, the effects of forward flight are not confined to changes in the mass flux through the rotor. There is also the well-known non-uniformity in the fore-aft distribution of inflow (i.e. non-zero  $\nu_c$ ), even in the absence of an aerodynamic pitching moment. The effect can be expressed in either of the following two forms:

$$\nu_c = K_c \nu_o \quad (6)$$

$$2V\nu_c = K_c C_T \quad (7)$$

The former expression is typically favored whenever the effect is calculated using a vortex theory while the latter expression results from the actuator disc (linearized potential theory) point of view. Provided the flight speed is high enough that  $V_G \approx V$  and the momentum expression for  $\nu_o$  is used, these two representations are equivalent and it remains only to consider the theories for  $K_c$ .

Many such theories have been proposed, with a summary [10] shown in Table 2. The simplest and most well-known of these, due to Coleman et al., is based on a linear geometric skewing of a constant-strength vortex tube wake, giving

$$K_c = \tan \frac{\chi}{2} \quad (8)$$

A more credible calculation was performed by Mangler and Squire [21]. By linearizing the incompressible Euler equations in high-speed steady flight, they obtained Laplace’s equation for the pressure field, which they solved using the Kinner functions to establish a specified distribution of pressure difference across the disc. Mangler and Squire considered a pressure distribution which results in thrust only (no moments). The perturbations in fluid velocity were calculated by integration of the pressure gradient along lines which are parallel to the freestream. The result, which they carefully and correctly stated applies only for lightly loaded rotors ( $C_T/V^2 \ll 1$ ), is:

$$K_c = \frac{15\pi}{32} \sqrt{\frac{1 + \sin \alpha}{1 - \sin \alpha}} \quad (9)$$

AUTHOR	$K_c$	$\left. \frac{dK_c}{d\chi} \right _{\chi=0}$
Coleman	$\tan \frac{\chi}{2}$	$1/2 = 0.500$
Drees	$\frac{4}{3} \tan \frac{\chi}{2}$	$2/3 = 0.667$
Payne	$\frac{\frac{4}{3} \tan \chi}{\frac{5}{8} + \tan \chi}$	$10/9 = 1.111$
Blake	$\sqrt{2} \sin \chi$	$\sqrt{2} = 1.414$
Pitt	$\frac{15\pi}{32} \tan \frac{\chi}{2}$	$15\pi/64 = 0.736$
Howlett	$\sin^2 \chi$	0
AVERAGE	N/A	0.738

Table 2: Models for First Harmonic Inflow Due to Wake Skewing (Following Table 2 in [10]. Drees dependence on  $\mu$  omitted for simplicity.)

It must be emphasized that  $\alpha$  is the disc angle of attack.

The Pitt model, as originally reported [9], was a direct extension of the Mangler-Squire result to incorporate pressure distributions which give rise to pitch and roll moments. The result may be expressed in the same form as the momentum theory, with Equation (4) replaced in high-speed flight by

$$[J] = V \begin{bmatrix} \frac{-4 \sin \alpha}{\gamma_i^2 + (\gamma_i^2 - 2) \sin \alpha} & 0 & \frac{\gamma_i \cos \alpha}{\gamma_i^2 + (\gamma_i^2 - 2) \sin \alpha} \\ 0 & \frac{\sin \alpha - 1}{4} & 0 \\ \frac{\gamma_i \cos \alpha}{\gamma_i^2 + (\gamma_i^2 - 2) \sin \alpha} & 0 & \frac{(\sin \alpha - 1)/2}{\gamma_i^2 + (\gamma_i^2 - 2) \sin \alpha} \end{bmatrix} \quad (10)$$

where  $\gamma_i \equiv 15\pi/64$ . Note that the Pitt model is linear in both the inflow velocities and the thrust and moments.

Subsequent modifications of the original Pitt model amounted more or less to the incorporation of two observations, both of which were contemplated in the original paper [9, page 33]. First, since  $\chi = 90^\circ + \alpha$  in forward flight, it is possible to rewrite Equation (10) as

$$[J] = V \begin{bmatrix} \frac{4 \cos \chi}{\gamma_i^2 + (2 - \gamma_i^2) \cos \chi} & 0 & \frac{\gamma_i \sin \chi}{\gamma_i^2 + (2 - \gamma_i^2) \cos \chi} \\ 0 & \frac{-(1 + \cos \chi)}{4} & 0 \\ \frac{\gamma_i \sin \chi}{\gamma_i^2 + (2 - \gamma_i^2) \cos \chi} & 0 & \frac{-(1 + \cos \chi)/2}{\gamma_i^2 + (2 - \gamma_i^2) \cos \chi} \end{bmatrix} \quad (11)$$

Second, if  $V$  in the Pitt calculations is replaced by a general mass flow parameter, similar to the Glauert

expression, a universal theory (applicable from hover through high speed flight at arbitrary disc angle) results.

For a rotor generating only thrust, the third row of the  $[J]$  matrix given by Equation (11) is equivalent<sup>3</sup> to Equation (7) with

$$K_c = 2\gamma_i \tan \frac{\chi}{2} \quad (12)$$

Thus, the modified Pitt model recovers the functional form of Coleman et al. for the relationship between  $K_c$  and  $\chi$ . (It will be convenient for further comparisons to define  $\bar{K}_c$  as the value of  $K_c$  at  $\chi = 90^\circ$ ; Coleman has  $\bar{K}_c = 1$ , while the modified Pitt model has  $\bar{K}_c = 2\gamma_i = 1.47$ .)

It should be noted that while the replacement of the disc angle with the wake skew angle is perfectly acceptable at high speed, extension of the functional form of  $[J]$  to near-hover flight conditions based on this substitution does not carry with it the analytical rigor of the original Pitt model. Furthermore, the complicated mass-flow parameter is, like the Glauert value, essentially a conjecture which satisfies the limiting conditions. Therefore, both of these changes must be validated through the demonstration of improved correlation with experimental data.

#### 4.2.4 Non-Axial Flight: Applications

The first issue to be considered is the prediction of the uniform portion of the induced velocity using momentum theory with the Glauert mass flow parameter. Based on the data summarized in [10], the theory seems to be reasonably good at low forward speeds ( $C_T/V^2 \geq 2$ ), but becomes quite poor at advance ratios exceeding about 0.2 (see, e.g., Figures 13 and 34 and Table 4 in [10]).

The consequences of the steady cosine harmonic inflow due to thrust have been known for some time, and were substantiated with the well documented measurements reported in [22]. Because the rotor responds approximately 90-degrees out-of-phase to the aerodynamic inputs, the fore-aft variation in induced velocity causes a pronounced change in the lateral flapping. The theory focuses our efforts to quantify this effect on functional form of the relationship between  $K_c$  and the wake skew angle,  $\chi$ . Unfortunately, there is very little information in the literature which allows firm conclusions to be drawn, largely because of the very rapid increase in the wake skew angle with advance ratio for rotors with typical disc loading [23]. For example, of all the data summarized in [10], the smallest non-zero wake skew angle is 61 degrees, and

<sup>3</sup> $\sin \chi / (1 + \cos \chi) \equiv \tan \chi / 2$

this occurs at an advance ratio of only 0.067! Therefore, using these data to evaluate the proposed functional forms of  $K_c$  given in Table 2 is not realistically possible. Indeed, the evaluation in [10], based on an overall impression from the data, suggests only that the Coleman value of  $\bar{K}_c$  is too small by a factor of about 2, implying that the Pitt value is too small by about 36 percent.

Similar difficulties hinder verification of the complex functional forms of the elements of the  $[J]$  matrix in the modified Pitt model. The most well known validation [24] includes comparisons to forward flight data for a wake skew angle of 90 degrees only. (All of the data are for an unlifting rotor at zero disc angle.) Therefore, the comparisons provide no validation of the modifications to the original Pitt model. Nevertheless, the data do enable a comparison of the quite different structures of the original Pitt and momentum  $[J]$  matrices for edgewise flow (EF):

$$[J]_{EF_{Pitt}} = \mu \begin{bmatrix} 0 & 0 & \frac{1}{\gamma_i} \\ 0 & -\frac{1}{4} & 0 \\ \frac{1}{\gamma_i} & 0 & -\frac{1}{2\gamma_i^2} \end{bmatrix} \quad (13)$$

$$[J]_{EF_{mom}} = \mu \begin{bmatrix} 2 & 0 & 0 \\ 0 & -\frac{N}{2} & 0 \\ 0 & 0 & -\frac{N}{2} \end{bmatrix} \quad (14)$$

Because of the known importance of the fore-aft inflow variation for a thrusting rotor, which is not included in the momentum theory, a third theory of interest, which we will refer to as the modified momentum theory, replaces the (3,1) element of the  $[J]_{EF_{mom}}$  matrix with  $\bar{K}_c N/2$ , using  $\bar{K}_c = 2$ , as suggested by [10].

With these three inflow models, the comparisons with test data presented in [24] are revisited here. The complete 9-state dynamic model used for the calculations is detailed in the Appendix. Comparisons are presented only for those cases where the most significant differences between the momentum and Pitt models are evidenced, namely selected static roll moment control derivatives and the frequency response of roll moment to collective pitch [24, Figures 9 and 12]. The main objective is to establish the extent to which shortcomings in the momentum theory are due to the omission of the wake skewing effect.

Shown in Figure 4 is a comparison of the predicted and measured values of  $\frac{\partial(C_L/a\sigma)}{\partial\vartheta}$  presented as a function of advance ratio. From basic notions of lifting rotor response to forward speed, one generally expects the rotor to flap back and to the right, so that the rolling moment would be expected to be positive and increasing with  $\mu$ . However, the large flapping frequency (1.17) and low Lock number (4.2) of

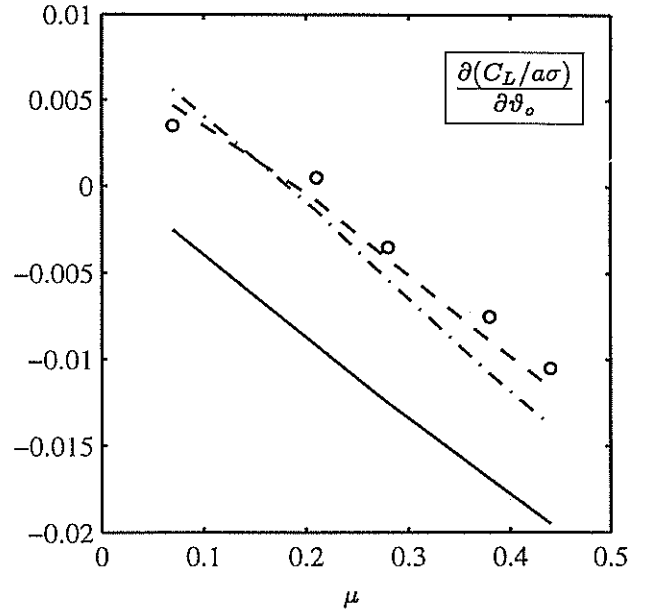


Figure 4: Steady Roll Moment Response to Collective Pitch Inputs, after Figure 9a in [24]. Solid Line = Momentum; Dashed Line = Pitt; Dot-Dashed Line = Modified Momentum.  $\gamma = 4.2$ ,  $\bar{K}_\beta = 0.369$ ,  $\mu = 0.36$ ,  $a\sigma = 0.79$ .

this rotor significantly reduce from 90° the phase difference between applied moments and rotor flap response. Thus, the nominal lateral response to collective pitch, predicted with momentum theory, is flapping to the left, with a resulting negative rolling moment. Given the well known dependence of lateral flapping on  $\nu_c$ , it is not surprising that momentum theory alone ( $\bar{K}_c = 0$ ) shows poor correlation with the data. That the Pitt model shows slightly better agreement with the data than the modified momentum theory, despite the fact that the Pitt value of  $\bar{K}_c$  is only 1.47, is the result of the structure of the Pitt  $[J]$  matrix. In the momentum theory with wake skewing, the pitching moment which accompanies the longitudinal flapping in forward flight reduces the cosine inflow harmonic substantially, resulting in the need for a much larger value of  $\bar{K}_c$  to match the flight data. The Pitt model, on the other hand, predicts that aerodynamic pitching moments affect only the uniform inflow, so that the cosine inflow due to thrust is not reduced. Although this conclusion is based only on a simple calculation and comparison to only one data set, it seems that previous conclusions about the magnitude of the wake skewing effect (i.e. the value of  $\bar{K}_c$ ) may need to be revised if they were based on calculations performed with momentum theory.

Figure 5 shows the comparisons of  $\frac{\partial(C_L/a\sigma)}{\partial\vartheta}$ .

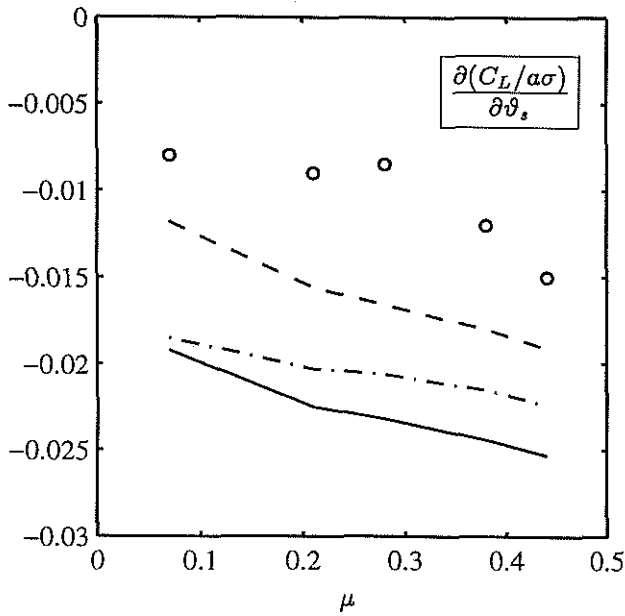


Figure 5: Steady Roll Moment Response to Longitudinal Cyclic Pitch Inputs, after Figure 9b in [24]. Legend and Numerical Values as in Figure 4

Though none of the models is adequate, the Pitt model fares best, with only a small part of the difference between Pitt and momentum being attributable to the wake skewing effect.

Finally, we turn attention to the dynamic case in forward flight, represented by the frequency response<sup>4</sup> shown in Figure 6 for an advance ratio of 0.36, which is representative of the data at other advance ratios [24, Figures 11, 13]. The momentum theory correlates quite poorly with the data. Except for small differences in magnitude for frequencies below 0.1 per rev, the Pitt and modified momentum models are quite similar and correlate reasonably well with the test data (though the log scaling makes the errors appear smaller than they are).

Mathematically, the effect of wake skewing appears as a change in the location of the zeros associated with the progressing cyclic flap mode. The Laplace transforms of the cyclic flapping equations with only collective pitch inputs are

$$(s^2 + \frac{\gamma}{2}\Gamma_3 s + \bar{K}_\beta)a_{1s} + (2s + \frac{\gamma}{2}\Gamma_3 + \frac{\gamma}{8}\mu^2\Gamma_1)b_{1s} = \frac{\gamma}{2}\mu\Gamma_2 a_o + \frac{\gamma}{2}\Gamma_3 \nu_c \quad (15)$$

<sup>4</sup>The traditional logarithmic scaling employed here reveals the differences between the theories and the data quite starkly. The correlation between the Pitt model and the data here appears somewhat better than in [24, Figure 12]; see the Appendix for a possible explanation.

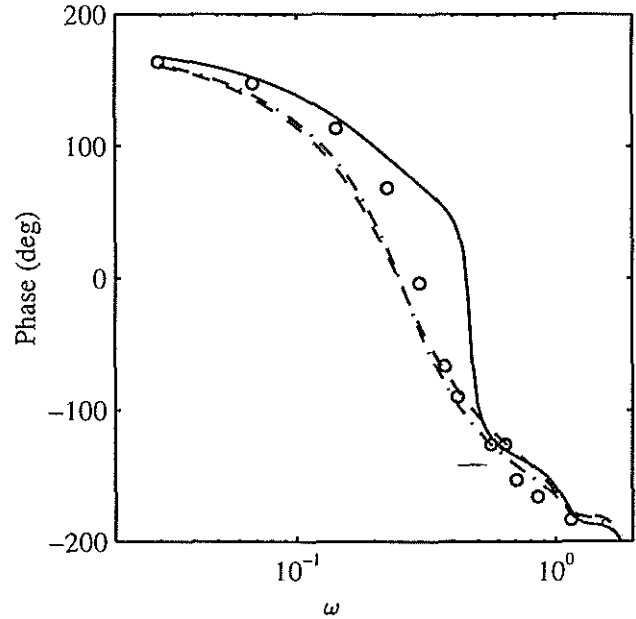
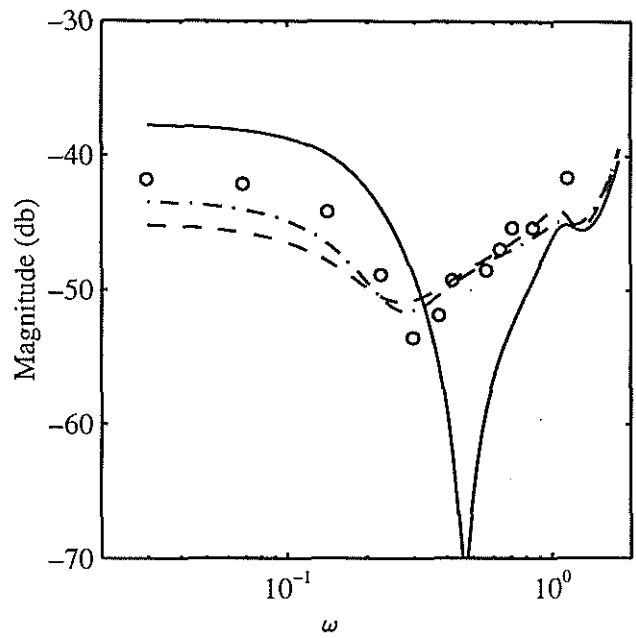


Figure 6: Frequency Response of Roll Moment to Collective Pitch Inputs ( $\frac{\partial(C_L/a\sigma)}{\partial\vartheta_o}$ ) after Figure 12 in [24]. Legend as in Figure 4.  $\gamma = 4.25$ ,  $\bar{K}_\beta = 0.3225$ ,  $\mu = 0.36$ ,  $a\sigma = 0.79$ .

$$-(2s + \frac{\gamma}{2}\Gamma_3 - \frac{\gamma}{8}\mu^2\Gamma_1)a_{1s} + (s^2 + \frac{\gamma}{2}\Gamma_3 s + \bar{K}_\beta)b_{1s} = -\mu\gamma\Gamma_2 \vartheta_o + \frac{\gamma}{2}\mu\Gamma_1 \nu_o + \frac{\gamma}{2}\Gamma_3 \nu_s \quad (16)$$

The quantities on the right-hand side may be approximated by their quasi-static values (i.e. expressed in terms of  $a_{1s}$ ,  $b_{1s}$ , and their time derivatives, and

$\vartheta_o$ ). In high-speed flight, the locations of the flapping poles are found to change only slightly due to these substitutions, so that a reasonable approximation to the transfer function is obtained by simply replacing the right-hand sides of Equations (15, 16) with  $\kappa_c \vartheta_o$  and  $\kappa_s \vartheta_o$ , respectively, where  $\kappa_c$  and  $\kappa_s$  are constants. The zeros in the lateral flapping response to collective are thus somewhat naively approximated by

$$\kappa_s(s^2 + \frac{\gamma}{2}\Gamma_3 s + \bar{K}_\beta) + \kappa_c(2s + \frac{\gamma}{2}\Gamma_3 - \frac{\gamma}{8}\mu^2\Gamma_1) = 0 \quad (17)$$

The value of  $\kappa_s$  is generally negative, due mostly to the direct appearance of  $\vartheta_o$  in Equation (16). The value of  $\kappa_c$  is generally positive due to the positive response of coning angle to collective pitch; it is made significantly more positive by the cosine inflow if the wake skewing effect is included in the calculation. A sketch of the variation of the zero locations as  $\kappa_c$  increases is shown in Figure 7. For rotor parameters corresponding to the data of Figure 6, it turns out that the value of  $\kappa_c$  due to coning ( $\frac{\gamma}{2}\mu\Gamma_2 a_o$  in Equation (15)) places the zeros almost exactly on the imaginary axis (solid circles in Figure 7). Addition of the wake skewing ( $\frac{\gamma}{2}\Gamma_3 \nu_c$  in Equation (15)) increases  $\kappa_c$ , moving the zeros well into the right-half plane (open circles in Figure 7). Therefore, the momentum theory shows a near zeroing of the roll moment response at a frequency of about 0.5 per-rev, while the theories which include the wake skewing (both modified momentum and Pitt) show a smoother variation in the magnitude. Note that the phase curves are quite sensitive to the precise location of the zeros with respect to the imaginary axis; calculations in [24] place the zeros of the momentum model just barely in the left-half plane, causing a misleading change in the shape of the phase curve.

### 4.3 Coupled Inflow-Rotor-Body Dynamics

The ultimate motivation for considering dynamic inflow for flight dynamics applications is the potential impact it has on the prediction of fuselage response to control inputs. The most direct approach for computing these effects is to increase the number of dynamic states to accommodate the inflow equations in the form of Equation (2), with the  $[J]$  matrix, taken either from the momentum theory or the Pitt model, evaluated in trim. The calculation of rotor loads must also be modified to reflect the presence of the non-constant induced velocity. We will begin with a discussion of results based on this direct approach and then describe some more recent results using a different implementation.

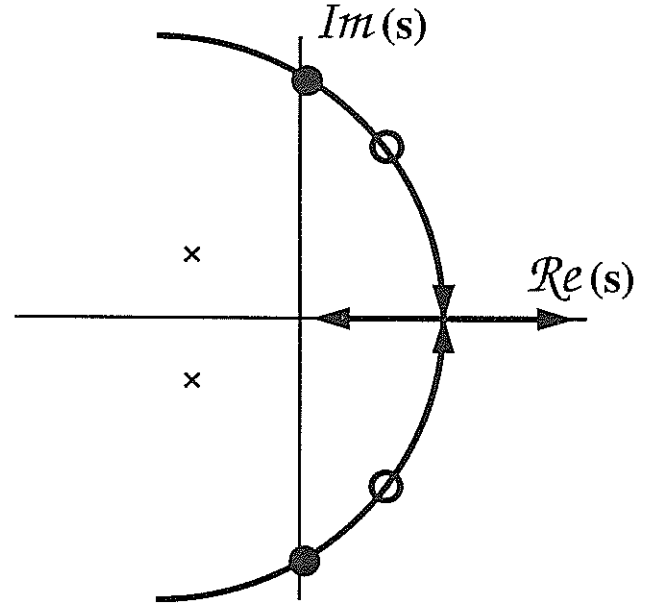


Figure 7: Approximate Variation in Lateral Flapping to Collective Pitch Zero Locations with  $\kappa_c$ . Solid Circle = Momentum; Open Circle = Modified Momentum;  $\times$  = Regressing Flap Poles.

#### 4.3.1 Some Fundamental Results

The effects of unsteady uniform inflow on the vertical acceleration response to collective pitch inputs in hover were examined in [25]. The thrust overshoot observed in the shaft-fixed experiments [15] becomes a vertical acceleration overshoot in free flight. The overshoot is not predicted by either the quasi-steady inflow or the no-inflow models, but is well described by the momentum theory.

Concerning the importance of dynamic harmonic inflow, [12] presents a simple 3-degree of freedom model for the coupled dynamics of the inflow, rotor and fuselage. The results indicate that the inflow time response is of increased importance for stiff rotors (i.e. large equivalent hinge offset). This is consistent with the increased coupling between the rotor and body modes which results from the higher control power of a stiff rotor. The paper also shows that models which include flapping dynamics must also include inflow dynamics to obtain a consistent representation, although no flight test data are available to firmly establish the correct time constants. Concerning the value of the wake rigidity factor, [12] shows that it can significantly impact the time response, and [26] finds improved correlation with flight data for  $N = 1$  (rigid wake).

There is a conspicuous lack of fundamental investigations concerning the effects of dynamic inflow on

control response in forward flight. The effects are generally expected to diminish as forward speed increases, but no definitive conclusions are available.

#### 4.3.2 Wake Distortion Effects

Incorporating dynamic inflow, the theory for which is based on a steady, translational flight condition, into a flight dynamics model warrants closer attention. If Equation (2) is properly linearized, consideration must be given to perturbations in the  $[J]$  matrix. The nature of these  $[J]$  perturbation terms can be seen by considering the wake skewing effect in near-hovering flight, where the wake skew angle will be small ( $\chi \approx u_h/\nu_o$ ), and the effect can be represented as

$$\nu_c = \nu_o \bar{K}_c \tan \frac{\chi}{2} \approx \nu_o \bar{K}_c \frac{u_h}{2\nu_o} = \frac{\bar{K}_c}{2} u_h \quad (18)$$

Similarly,  $-\nu_h$  leads to  $\nu_s$ . More generally, with an arbitrary functional form for  $K_c$ , we have

$$\nu_c = \left. \frac{dK_c}{d\chi} \right|_{\chi=0} u_h \quad (19)$$

The conclusion of Section 4.2.4 was that the functional form of  $K_c$  is only very poorly known, with considerable uncertainty surrounding even the value of  $\bar{K}_c$ . Indeed, the difficulty of assigning a meaningful value to  $dK_c/d\chi$  can be seen in Table 2, where each of the six theories for calculating  $K_c$  gives a different value of the derivative, ranging from identically zero to 1.41, with a mean value of 0.738 and a standard deviation of 0.45. Based on this uncertainty, it is perhaps best to consider alternative means of including these terms in the inflow equations.

Recently, a prescribed vortex wake calculation was used to show that there are additional wake distortion terms due to hub pitch and roll rates [27]. These effects are large in hover but rapidly diminish with forward speed. The momentum formulation of the harmonic inflow equations in hover can be rewritten ("extended momentum theory") to explicitly include all the distortion terms:

$$\tau \dot{\nu}_c + \nu_c = -\frac{2}{N\nu_o} C_M + K_T u_h + K_R (q + \dot{a}_{1s}) \quad (20)$$

$$\tau \dot{\nu}_s + \nu_s = -\frac{2}{N\nu_o} C_L - K_T v_h + K_R (p - \dot{b}_{1s}) \quad (21)$$

where  $\tau = \frac{32}{45\pi N\nu_o}$  and the values of  $K_T$  and  $K_R$  are of order unity in hover.

Figure 8 and Figure 9 show comparisons with flight test data of the on- and off-axis responses, respectively, of body rate to lateral cyclic pitch for the

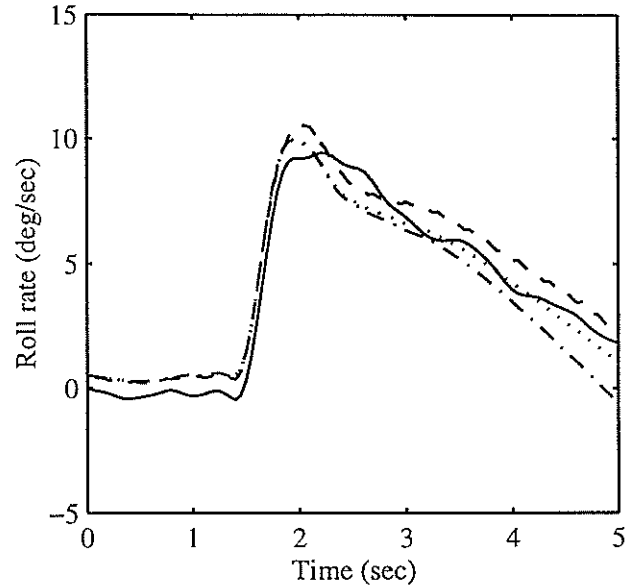


Figure 8: Effect of  $K_T$  and  $K_R$  on Body Roll Rate Response to Lateral Cyclic Inputs (On-Axis); Solid Line = Flight Data; Dotted Line = Momentum Theory; Dot-Dashed Line = Momentum + Translation; Dashed Line = Momentum + Translation + Rotation (Extended Momentum Theory).  $K_T = 15\pi/64$ ,  $K_R = 2.3$  (best fit to data).

UH-60 in hover, predicted with the momentum theory, Equation (2), and with the extended momentum theory, Equations (20, 21). The wake distortion effects have only a small impact on the (already well-predicted) on-axis response, but they have a dramatic impact on the off-axis response, with incremental improvements offered by both the translational and rotational effects. Note that only by including the rotational effects ( $K_R$ ) is it possible to obtain the correct initial (high frequency) off-axis response.

That the value of  $K_R$  giving the best match to the test data is much larger than the theoretical value is consistent with other studies [1]; additional research is being performed to provide a more rigorous analytical foundation for the calculation of the wake distortion parameters,  $K_T$  and  $K_R$ . The main conclusion to be drawn from the simple analysis is that the parameters are of order unity and that the effects of wake distortion have a pronounced impact on the off-axis control response.

The wake distortion effects due to shaft translation and rate cannot be recovered in a simple way from the Pitt model. The attempt in [28] to present a non-linear version of the Pitt theory incorporating shaft motion effects has several deficiencies. The claim

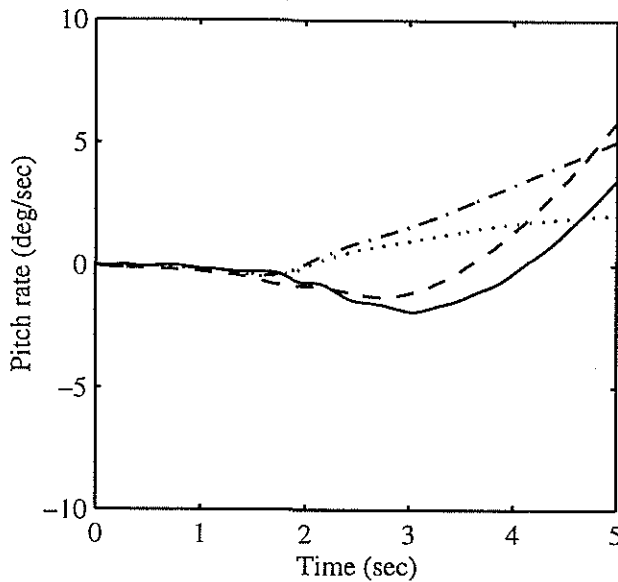


Figure 9: Effect of  $K_T$  and  $K_R$  on Body Pitch Rate Response to Lateral Cyclic Inputs (Off-Axis); Lines and Values as in Figure 8.

that the Pitt model formally applies in wind axes is not correct for unsteady flight conditions. Consider for example a rotor in forward flight generating only thrust. The steady inflow in this case would consist of uniform and cosine harmonic components. Suppose the rotor shaft were acted on by an impulsive force, instantaneously changing its direction of motion by 90 degrees (i.e. to sideslip at the same speed) in the shaft frame of reference. From the wind axis perspective, there has been no change, so the wind-axis inflow components would be unchanged. Therefore, in the shaft azimuth, the cosine harmonic would instantaneously vanish while the sine harmonic would instantaneously acquire a steady value. This is clearly not the expected physical response, which would more realistically be represented by a first-order time constant<sup>5</sup>. From a more practical point of view, their generalization of the Pitt model fails because the angle between the shaft axes and the wind axes (their  $\Delta$  angle) is not defined in hover, making the perturbation formulation in terms of changes to this angle inherently ill-posed for the flight condition where these effects are most important.

<sup>5</sup> Derivations in [28] actually do introduce a first-order time lag in the response to changes in wind direction by omitting the  $[\dot{T}]$  term in their Equation (23). An attempt to incorporate the Pitt model in a nonlinear simulation using wind axes (without the analytical omission of the  $[\dot{T}]$  term) showed unrealistic and rapid changes to the shaft-azimuth harmonic inflow components due to shaft velocities [29].

## 5 Vortex Theories and Harmonic Loading

This section considers the relationship between the vortex and actuator disc (momentum) theories in the case of first harmonic loading.

Considering the hovering case, the aerodynamic roll and pitch moments on the rotor can be found from blade element theory:

$$C_M = C_{M,qs} + \frac{a\sigma}{16}\nu_c \quad (22)$$

$$C_L = C_{L,qs} + \frac{a\sigma}{16}\nu_s \quad (23)$$

where  $( )_{qs}$  is used to denote the “quasi-steady” moments which depend only on the geometric angle of attack of the blade and the flapping motion (independent of the induced velocity). To complete the analysis, it is necessary to relate the induced velocity components to the blade loading, which can be done using the actuator disc (momentum) theory of Equation (2). The result can be used to define the steady-state lift deficiency function

$$C = \frac{C_M}{C_{M,qs}} = \frac{C_L}{C_{L,qs}} = \frac{1}{1 + \frac{a\sigma}{8N\nu_c}} \quad (24)$$

If  $a$  and  $N$  are respectively chosen as  $2\pi$  and 1, this result is equivalent to the zero-reduced-frequency limit of the Loewy lift deficiency function since the forcing frequency is equal to the rotor rotation rate [30, 9]. This agreement is somewhat remarkable in light of the fact that the Loewy result is based on a two-dimensional vortex theory while the actuator disc result follows from a three-dimensional analysis.

This unexpected agreement between the two distinct approaches can be clarified by examining the work of Miller [31] who treated this problem using a three-dimensional vortex model. Considering the case of first harmonic blade loading (i.e. bound blade circulation is a first harmonic in blade azimuth), the induced velocity at the rotor was computed by integrating both shed and trailing wake vorticity components, where the shed wake was properly truncated to account for finite blade radius. The bound circulation is also directly related to the blade aerodynamic loading, giving a complete theory. In the limit of a rotor with infinitely many blades, which is analogous to the actuator disk assumption, the resulting lift deficiency function is identically equal to that given by Equation (24). Thus, the contribution of the trailing vortices is equal and opposite to the change brought about by truncating the shed vorticity, so that Loewy’s 2D theory gives the correct result.

In Miller's original analysis, the vorticity is convected downstream at the mean induced velocity (rigid wake), so that  $N = 1$ ; it can be shown that the effect of including harmonic inflow terms in the vorticity convection (non-rigid wake) results in  $N = 2$ . Although the analysis assumed that the circulation was independent of radius, it can also be shown that a radial variation in bound circulation will only affect the induced velocity distribution but will not change the resulting lift deficiency function.

The equivalence of the steady three-dimensional vortex theory and the steady actuator-disc (momentum) theory gives credence to the extended momentum formulation discussed in Section 4.3.2. Although the wake distortion effects were calculated with a simple vortex theory, it is reasonable to suppose, in light of the present discussion, that these effects may properly be superimposed with the usual dynamic inflow calculations. Conceptually, we observe that unsteady momentum theory computes the induced velocity due to azimuthal variations in blade circulation with the shaft fixed, while the wake distortion vortex theory computes the induced velocity variation resulting from constant circulation but allowing tip-path plane translation and rotation. Therefore, extended momentum theory, which directly superimposes these two effects, can be viewed as a linearized, physical wake model for a rotorcraft in flight.

It should be noted that this section has considered only the steady response to harmonic loading. Based on the results of Section 3, we expect that there may be additional effects resulting from the unsteady relationship between local angle of attack and local blade lift. Most notably a lag in the response of the blade lift may result in a phase lag in the response of the rotor which cannot be obtained with the usual dynamic inflow theory which produces a lead in the rotor response. As discussed above, an adequate representation of these effects for the harmonic loading case is under investigation.

## 6 Conclusions

- A complete unsteady vortex theory was shown to be equivalent to a combination of unsteady blade element theory and unsteady actuator disc (momentum) theory. Most flight-dynamics applications employ quasi-static blade element theory and dynamic inflow theory, which was shown to be equivalent to neglecting the high-frequency dynamics of the 2D shed vorticity. This low-frequency approximation may need to be reexamined in light of evidence which suggests the

neglected effects are of greater importance at high Mach number.

- The original Pitt model is better able to predict the control response of an isolated rotor in an edgewise flight condition than the momentum theory. Addition of the wake skewing (Coleman) effect to the momentum theory improves the predictions, but, based on a limited comparison with test data, does not appear to render them as accurate as the Pitt model.
- Wake distortion terms due to hub velocity and angular rate have a significant impact on the prediction of off-axis response of body rate to cyclic inputs in near-hover flight conditions. The Pitt model cannot be readily modified to include these effects.
- The values of the constants used to represent wake distortion effects in the extended momentum theory are not well known either in theory or from test data. More research is necessary.
- The extended momentum formulation is further justified in light of the equivalence of vortex and momentum theories for predicting the steady rotor response to first harmonic loading.

## References

- [1] M. Hossein Mansur and Mark B. Tischler. An empirical correction method for improving off-axis response prediction in component-type flight mechanics helicopter models. In *AGARD Flight Vehicle Integration Panel Symposium on Advances in Rotorcraft Technology*, Ottawa, Canada, May 1996.
- [2] Jay W. Fletcher. Identification of linear models of the UH-60 in hover and forward flight. In *Proceedings of the Twenty-First European Rotorcraft Forum*, St. Petersburg, Russia, August 1995.
- [3] T. Theodorsen. General theory of aerodynamic instability and the mechanism of flutter. Report 496, NACA, 1935.
- [4] Theodore von Karman and W. R. Sears. Airfoil theory for non-uniform motion. *Journal of the Aeronautical Sciences*, 5(10):379-390, August 1938.
- [5] William R. Sears. Operational methods in the theory of airfoils in non-uniform motion. *Journal of the Franklin Institute*, 230:95-111, 1940.

- [6] R. T. Jones. The unsteady lift of a wing of finite aspect ratio. Report 681, NACA, 1940.
- [7] B. Mazelsky. Numerical determination of indicial lift of a two-dimensional sinking airfoil. Technical Note 2562, NACA, December 1951.
- [8] W. F. Ballhaus and P. M. Goorjian. Computation of unsteady transonic flows by the indicial method. *AIAA Journal*, 16(2), February 1978.
- [9] Dale M. Pitt and David A. Peters. Theoretical prediction of dynamic-inflow derivatives. *Vertica*, 5:21-34, 1981.
- [10] Robert N. Chen. A survey of nonuniform inflow models for rotorcraft flight dynamics and control applications. *Vertica*, 14(2):147-184, 1990.
- [11] Alfred Gessow and Garry C. Myers, Jr. *Aerodynamics of the Helicopter*. Frederick Ungar Publishing Co., New York, 1952.
- [12] H. C. Curtiss, Jr. Stability and control modelling. *Vertica*, 12(4):381-394, 1988.
- [13] L. M. Milne-Thomson. *Theoretical Aerodynamics*. MacMillan and Company, Ltd., London, 2 edition, 1952.
- [14] A. R. S. Bramwell. *Helicopter Dynamics*. Edward Arnold Publishers, Ltd., London, 1976.
- [15] Paul J. Carpenter and Bernard Fridovich. Effect of a rapid blade-pitch increase on the thrust and induced-velocity response of a full-scale helicopter rotor. Technical Note 3044, National Advisory Committee for Aeronautics, November 1953.
- [16] H. C. Curtiss, Jr. and Norman K. Shupe. A stability and control theory for hingeless rotors. In *American Helicopter Society Twenty-Seventh Annual Forum Proceedings*, Washington, DC, May 1971.
- [17] Kurt H. Hohenemser and S. T. Crews. Model tests on unsteady rotor wake effects. *Journal of Aircraft*, pages 58-60, January 1973. Technical Note.
- [18] S. T. Crews, Kurt H. Hohenemser, and Robert A. Ormiston. An unsteady wake model for a hingeless rotor. *Journal of Aircraft*, pages 758-760, December 1973. Technical Note.
- [19] D. Banerjee et al. Identification of state variables and dynamic inflow from rotor model dynamic tests. *Journal of the American Helicopter Society*, 22:28-36, April 1977.
- [20] D. Banerjee et al. Parameter identification applied to analytic hingeless rotor modeling. *Journal of the American Helicopter Society*, 24:26-32, January 1979.
- [21] K. W. Mangler and H. B. Squire. The induced velocity field of a rotor. Reports and Memoranda 2642, R.A.E., May 1950.
- [22] F. D. Harris. Articulated rotor blade flapping motion at low advance ratio. *Journal of the American Helicopter Society*, 17, January 1972.
- [23] Robin B. Gray. *An Aerodynamic Analysis of a Single-Bladed Rotor in Hovering and Low-Speed Forward Flight as Determined from Smoke Studies of the Vorticity Distribution in the Wake*. PhD thesis, Princeton University, Princeton, NJ, September 1956.
- [24] Gopal H. Gaonkar and David A. Peters. Effectiveness of current dynamic-inflow models in hover and forward flight. *Journal of the American Helicopter Society*, 31:47-57, April 1986.
- [25] Robert T. N. Chen and William S. Hindson. Influence of high-order dynamics on helicopter flight-control system bandwidth. *AIAA Journal of Guidance, Control, and Dynamics*, 9(2):190-197, March 1986.
- [26] Mark G. Ballin and Marie-Alix Dalang-Secretan. Validation of the dynamic response of a blade-element UH-60 simulation model in hovering flight. *Journal of the American Helicopter Society*, 36:77-88, October 1991.
- [27] Jeffrey D. Keller. An investigation of helicopter dynamic coupling using an analytical model. In *Proceedings of the Twenty-First European Rotorcraft Forum*, St. Petersburg, Russia, August 1995. Lichten Award Paper.
- [28] David A. Peters and Ninh HaQuang. Dynamic inflow for practical applications. *Journal of the American Helicopter Society*, 33:64-68, October 1988. Technical Note.
- [29] Uwe T. P. Arnold. Formulation of dynamic inflow in wind axes. Private Communication, 1995.
- [30] W. Johnson. *Helicopter Theory*. Princeton University Press, Princeton, NJ, 1980.
- [31] R. H. Miller. Rotor blade harmonic air loading. *AIAA Journal*, 2(7), 1964.

0	0	0	1	0	0	0	0	0
0	0	0	0	1	0	0	0	0
0	0	0	0	0	1	0	0	0
$-(\bar{K}_\beta + 1)$	0	0	$-\frac{\gamma}{2}\Gamma_3$	0	$\frac{\gamma}{4}\mu\Gamma_2$	$-\frac{\gamma}{2}\Gamma_2$	$-\frac{\gamma}{4}\mu\Gamma_2$	0
$\frac{\gamma}{2}\mu\Gamma_2$	$-\bar{K}_\beta$	$-\frac{\gamma}{2}(\Gamma_3 + \frac{\mu^2}{4}\Gamma_1)$	0	$-\frac{\gamma}{2}\Gamma_3$	-2	0	0	$\frac{\gamma}{2}\Gamma_3$
0	$\frac{\gamma}{2}(\Gamma_3 - \frac{\mu^2}{4}\Gamma_1)$	$-\bar{K}_\beta$	$\frac{\gamma}{2}\mu\Gamma_2$	2	$-\frac{\gamma}{2}\Gamma_3$	$\frac{\gamma}{2}\mu\Gamma_1$	$\frac{\gamma}{2}\Gamma_3$	0
0	0	0	$-\frac{\alpha\sigma}{2}\Gamma_2$	0	$\frac{\alpha\sigma}{4}\mu\Gamma_1$	$-\frac{\alpha\sigma}{2}\Gamma_1 - J_{1,1}$	$-\frac{\alpha\sigma}{4}\mu\Gamma_1 - J_{1,2}$	$-J_{1,3}$
0	$\frac{\alpha\sigma}{4}(\Gamma_3 - \frac{\mu^2}{4}\Gamma_1)$	0	$\frac{\alpha\sigma}{4}\mu\Gamma_2$	0	$-\frac{\alpha\sigma}{4}\Gamma_3$	$\frac{\alpha\sigma}{4}\mu\Gamma_1 - J_{2,1}$	$\frac{\alpha\sigma}{4}\Gamma_3 - J_{2,2}$	$-J_{2,3}$
$\frac{\alpha\sigma}{4}\mu\Gamma_2$	0	$-\frac{\alpha\sigma}{4}(\Gamma_3 + \frac{\mu^2}{4}\Gamma_1)$	0	$-\frac{\alpha\sigma}{4}\Gamma_3$	0	$-J_{3,1}$	$-J_{3,2}$	$\frac{\alpha\sigma}{4}\Gamma_3 - J_{3,3}$

Table 3: Flapping-Inflow Dynamic Model [F] Matrix.

0	0	0
0	0	0
0	0	0
$\frac{\gamma}{2}(\Gamma_3 + \frac{\mu^2}{2}\Gamma_1)$	0	$\frac{\gamma}{2}\mu\Gamma_2$
0	$-\frac{\gamma}{2}(\Gamma_3 + \frac{\mu^2}{4}\Gamma_1)$	0
$-\gamma\mu\Gamma_2$	0	$-\frac{\gamma}{2}(\Gamma_3 + \frac{3\mu^2}{4}\Gamma_1)$
$\frac{\alpha\sigma}{2}(\Gamma_2 + \frac{\mu^2}{2}\Gamma_0)$	0	$\frac{\alpha\sigma}{2}\mu\Gamma_1$
$-\frac{\alpha\sigma}{2}\mu\Gamma_2$	0	$-\frac{\alpha\sigma}{4}(\Gamma_3 + \frac{3\mu^2}{4}\Gamma_1)$
0	$-\frac{\alpha\sigma}{4}(\Gamma_3 + \frac{\mu^2}{4}\Gamma_1)$	0

Table 4: Flapping-Inflow Dynamic Model [G] Matrix.

## Appendix Rotor Model

The model used in the main text to describe the shaft-fixed coupled flapping-inflow dynamics is based on a centrally hinged, spring-restrained, untwisted rigid blade assumption, and is linearized about the non-lifting forward flight condition. The form of the model is

$$[D]\dot{x} = [F]x + [G]u \quad (25)$$

where  $x$  is

$$\left[ a_o \quad a_{1s} \quad b_{1s} \quad \dot{a}_o \quad \dot{a}_{1s} \quad \dot{b}_{1s} \quad \nu_o \quad \nu_s \quad \nu_c \right]^T \quad (26)$$

and  $u$  is

$$\left[ \vartheta_o \quad \vartheta_c \quad \vartheta_s \right]^T \quad (27)$$

The matrices are given in Table 3, Table 4, and Table 5. The aerodynamic integrals in the equations are defined by

$$\Gamma_n = \int_{e_A}^B r^n dr \quad (28)$$

Note that the assumption of centrally hinged blades (no kinematic hinge offset) will cause the flap damping to be incorrect. This is a possible source of small

differences between the present model predictions and those of [24].

For a centrally hinged, spring-restrained rotor, the normalized hub moment coefficients are expressed simply in terms of the cyclic flapping:

$$\frac{C_L}{a\sigma} = -\frac{\bar{K}_\beta}{2\gamma} b_{1s} \quad (29)$$

$$\frac{C_M}{a\sigma} = -\frac{\bar{K}_\beta}{2\gamma} a_{1s} \quad (30)$$

$$\begin{bmatrix} [J]_{3 \times 3} & [0]_{3 \times 3} & [0]_{3 \times 3} \\ [0]_{3 \times 3} & [J]_{3 \times 3} & [0]_{3 \times 3} \\ [0]_{3 \times 3} & [0]_{3 \times 3} & [M] \end{bmatrix}$$

Table 5: Flapping-Inflow Dynamic Model [D] Matrix.